ACS APPLIED MATERIALS & INTERFACES

Research Article

www.acsami.org

Femtosecond Laser-Induced Micropattern and Ca/P Deposition on Ti Implant Surface and Its Acceleration on Early Osseointegration

Chunyong Liang,*[,†] Hongshui Wang,[†] Jianjun Yang,[‡] Yanli Cai,[†,§] Xin Hu,[⊥] Yang Yang,[‡,#] Baoe Li,[†] Hongjie Li,[⊥] Haipeng Li,[†] Changyi Li,*[,⊥] and Xianjin Yang*[,§]

[†]School of Materials Science and Engineering, Hebei University of Technology, Tianjin 300130, China

[‡]Institute of Modern Optics, Nankai University, Tianjin 300071, China

[§]School of Materials Science and Engineering, Tianjin University, Tianjin 300072, China

[⊥]Stomatological Hospital, Tianjin Medical University, Tianjin 300070, China

[#]State Key Laboratory of Molecular Reaction Dynamics, Dalian Institute of Chemical Physics, Chinese Academy of Sciences, Dalian 116023, China

ABSTRACT: Surface microstructure and chemical composition of the implant are very important for its osseointegration in vivo. In this paper, a hierarchical micropattern covered with calcium phosphate (Ca/P phase) was obtained on titanium (Ti) implant surface by femtosecond lasers (FSL) irradiation in hydroxyapatite suspension. The hierachical micropattern as well as Ca/P phase increased osteoblastic cell adhesion. Higher expression of osteogenic markers (osteocalcin, osteopontin, and runt related transcription factor-2) on the surface treated by FSL of 2.55 J/cm^2 indicated the favorable effect of laser treatment on cell differentiation. In vivo studies were carried out to evaluate the effect of laser treatment and Ca/P deposition on the osseointegration. It showed that the binding capacity between bone and FSL-treated Ti implants was obviously stronger than that between bone and polished or sand blasting and acid etching (SLA) Ti implants. Bone trabecula surrounded the FSL-treated implants without fibrous tissue after 8-week implantation. Also, higher bone mineral density was seen surrounding the FSL-treated implants. Our in vitro and in vivo studies demonstrated that the FSL induced micropattern and Ca/P phase had positive effects on the acceleration of early osseointegration of Ti implants with bone tissue.

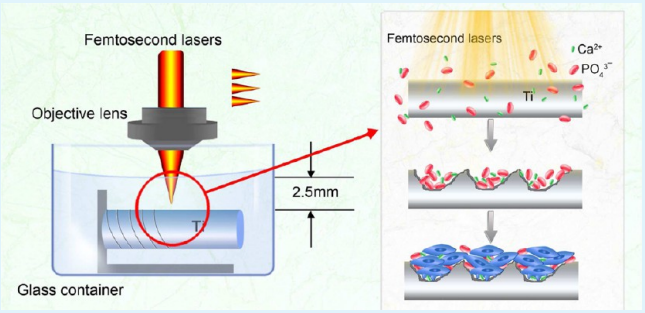

KEYWORDS: *femtosecond lasers, Ti implant, Ca/P phase, micropatterning, osseointegration*

INTRODUCTION

Titanium (Ti) and titanium alloys are widely used as hard tissue implant materials because of their excellent mechanical properties.[1] When the implant is permanently kept in a body, the integration between bone and implant is a great concern because better osseointegration can facilitate the early healing and relieve patients' pain.[2−4] However, metal materials usually have poor osseointegration, and thus the longevity of the metal implants is reduced. To tackle this problem, researchers have developed several methods to improve adhesion strength (osseointegration) between bone and implants, such as varying surface structure and chemical constituents.[5−8] Numerous in vitro and in vivo studies have shown that surface structure of titanium implants is important in determining the implant performance.[9−12] It has been reported that both microstructures[11,13] and nanostructures[10,14,15] influence biological processes at implant interfaces. In addition, when the nanostructure is formed on the implant surface, more adhesion positions are obtained for arginine-glycine-aspatic acid (RGD) sequence of extracellular matrix protein to enhance cell adhesion.[16,17] Ca^{2+} and PO_4^{3-} ions have advantages to the integration between specific protein of osteoblast and implant surface because they can induce ion supersaturation zone to improve the adhesion of osteoblast and secretion of extracellular matrix.[17]

It is ideal that the designed microstructure and Ca/P constituents are created simultaneously on the implant surface. However, it has not been reported so far. Usually, surface treatment was applied to obtain certain roughness, and then calcium phosphate coating formed through biomimetic mineralization. To achieve the simultaneous formation of designed microstructure and chemical constituents, laser technique has its own advantages. Referring to the literature, various surface structures have been obtained without pollution through the laser treatment on orthopedic implant surfaces,[6,7,18−24] which have positive effects on cell behaviors.[25] Compared with the ordinary long pulsed lasers, the femtosecond lasers (FSL) are more suitable for surface treatment of

Received: June 12, 2013
Accepted: July 25, 2013
Published: July 25, 2013

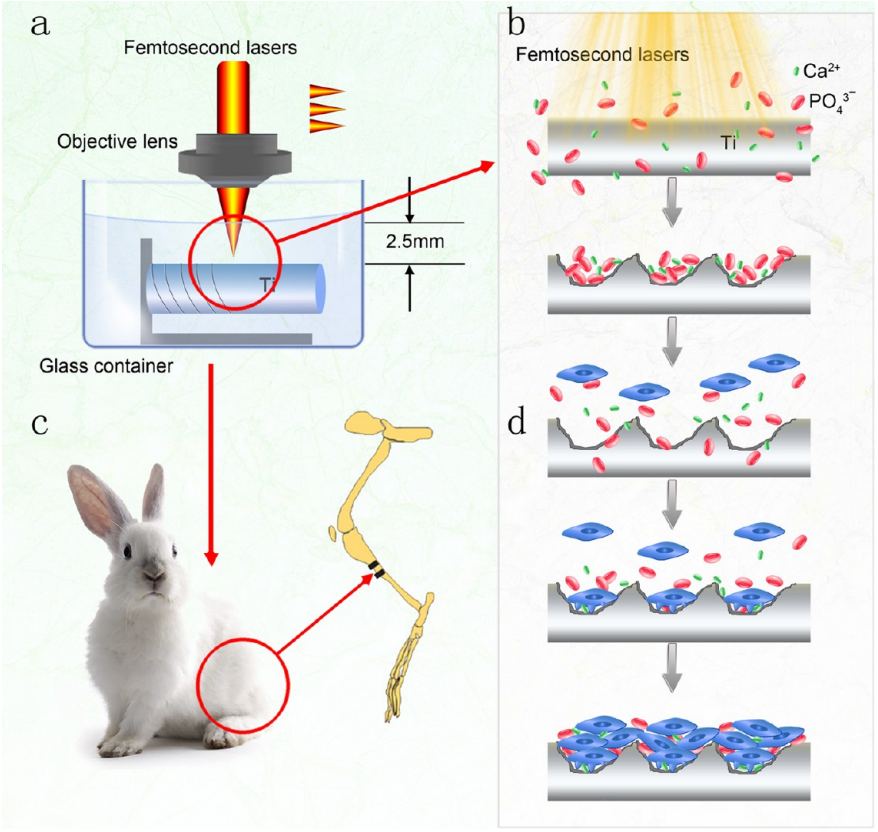

Figure 1. Process and mechanism of FSL treatment on titanium surface: (a) femtosecond laser ablation on the implant, (b) micropattern formation and Ca/P deposition, (c) in vivo process, (d) cell growth on the Ca/P deposited micropattern.

implants because of their advantages such as higher processing precision and lower heat affected zone. By adopting FSL irradiation and ablation, different surface structures could be processed on various solid materials.[21,26−29] Our previous studies also showed the feasibility[30−32] that a variety of surface patterns such as stripes, grooves, pores, as well as nanoparticles were obtained on pure Ti and NiTi alloy. Recently, FSL was employed to modify surface chemicals on Ti implants to form calcium alkali phosphate layer.[33,34] Photochemical reaction could be induced on the surface when it was treated in solvent along with the removable optical physics substances. During the reaction, ions and particles in the solvent were activated to bond with the implant materials.[35−37]

In this paper, FSL was utilized to induce micropattern and Ca/P deposition on the Ti implant surface simultaneously. As shown in Figure 1, the pure Ti surface was treated by near infrared FSL with different energies in calcium phosphate solution to obtain microstructures involving hierarchical roughness; meanwhile, Ca/P phase was coated on the pure Ti surface. The effect of microstructures and Ca/P phase on osteoblast behaviors was studied by in vitro cell culture test, and the influence of FSL treatment on early osseointegration of Ti implant was evaluated through in vivo rabbit model.

EXPERIMENTAL SECTION

Sample Preparation and Characterization. As described above in Figure 1, the pure Ti surface was treated by near infrared FSL, which was reported elsewhere.[35,36] The pure Ti sample in size of 10 mm × 10 mm ×1 mm was used during the in vitro experiment. After polished, samples were soaked in 2 mg/mL nano hydroxyapatite (HA, Beijing Dk Nano technology Co., LTD) suspension, and the solution/air interface was about 2.5 mm above the sample surface. With 50 fs in pulse width, 800 nm in centre wavelength and 1 kHz in repetition rate, infrared laser irradiated sample surface to induce micropatterns and Ca/P deposition on the surface. The other FSL parameters were set as: laser spot size about 100 μm, processing line distance of 100 μm, laser scanning speed of 0.2 mm/s, and laser processing monopulse energy at 100 and 200 μJ, respectively, which corresponded to energy flux of 1.27 and 2.55 J/cm^2. According to different laser pulse energy, the FSL-treated samples were marked as 100Ti and 200Ti. The control samples were pure Ti polished by 1200# abrasive paper (marked as Ti) and pure Ti treated by sand blasting and acid etching (marked as SLA).

Pure Ti stick, 2 mm in diameter and 6 mm in length, was used as implant in animal model. Firstly Ti stick of about 70 cm in length was installed in the processing system and immersed in 2 mg/mL nano HA suspension solution, and then FSL at the monopulse fluence of 2.55 J/cm^2 was used to process sample surface, and a nanosecond laser was used for cutting the stick into implants with 6 mm in length. Rotate speed and radial movement speed of FSL on implant surface were controlled according to the treatment process of Ti plates. All samples were kept in open air and sterilized in an autoclave at 121 °C for 20 min before the in vitro and in vivo tests.

The microstructures and chemical constituents were examined by scanning electron microscope (SEM, Hitachi S-4800) and energy spectrum (EDAX). Atom force microscope (AFM, Agilent 5500) was used to observe the three-dimensional microstructure of FSL-treated sample surface, which was also checked by transmittance electron microscope (TEM, Philips Tichnai 20). A little surface material was scraped gently and loaded on copper mesh, which was covered with carbon micro grid for TEM observation.

Cell Attachment Assay. MC3T3-E1 cells purchased from American Type Culture Collection (ATCC, Rockville, MD) were used to evaluate the osteoblastic cell response on various titanium surfaces. Cells were seeded on samples at a density of 2 × 10^4 cells/

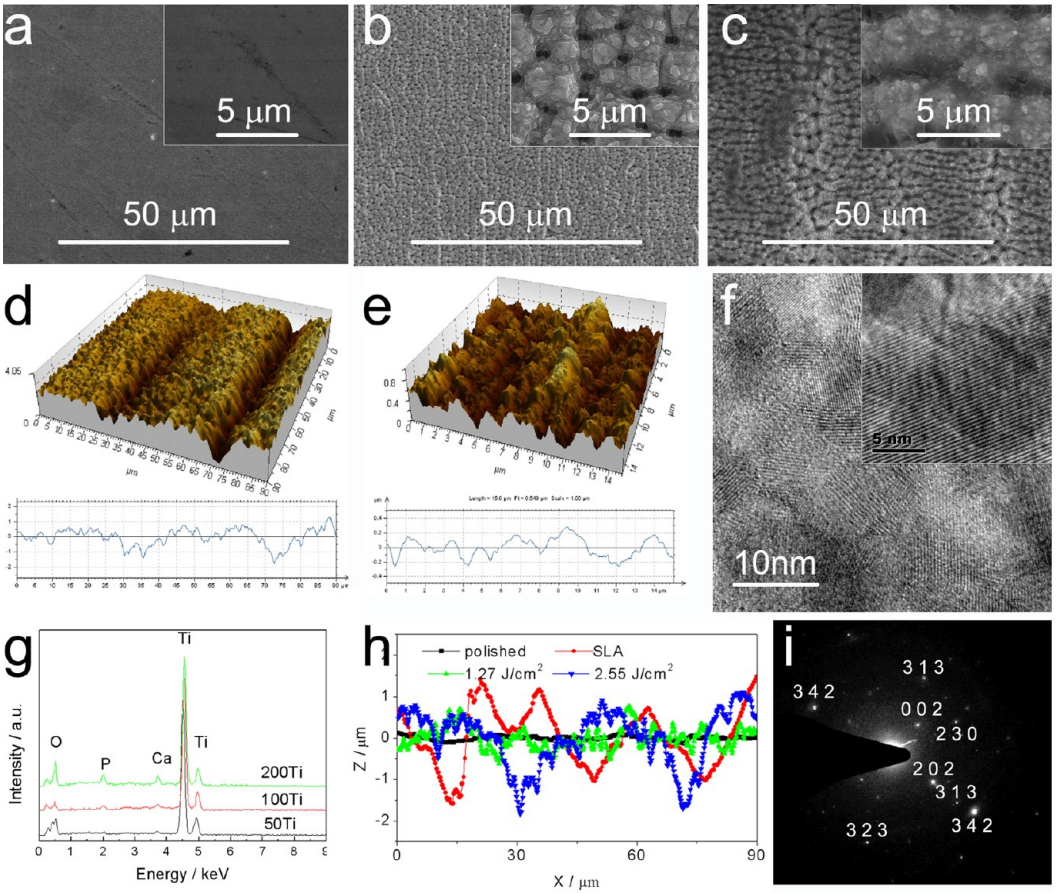

Figure 2. Surface analysis of femtosecond laser-treated samples: (a–c) SEM images of (a) polished Ti, (b) 100Ti, and (c) 200Ti; (d, e) AFM images of 200Ti; (f) TEM images of 200Ti; (g) EDAX profiles of samples; (h) profile curve of samples treated with different methods, (i) selected area electron diffractions of f.

cm^2 and then cultured at 37 °C in a 5% CO_2 incubator in a culture medium containing Dulbecco's Modified Eagle Medium (DMEM, GIBCO) supplemented with 10% fetal bovine serum (FBS, GIBCO) and 1% penicillin/streptomycin (Solarbio). After culturing for 12 h, the cells on Ti, 100Ti, 200Ti were rinsed with PBS, and then the adherent cells were detached by trypsinization and counted using a hemocytometer.

Osteoblast Cell Morphology. MC3T3-E1 cells were cultured on sample surfaces for 2 days at a density of 2×10^4 cells/mL, and then washed with PBS, and fixed by 4% paraformaldehyde for 20 min. For immunofluorescence imaging, the F-actin cytoskeleton of osteoblasts was stained with phalloidin–rodamine (Invitrogen) for 20-30 min, and the nucleus of cells were counterstained with 4′,6-diamidino-2-phenylindole (DAPI). Immunofluorescence images were taken by a fluorescence microscope (OLYMPUS X-81).

Real-Time PCR Analysis. Real time PCR analysis was performed after cells were cultured at the seeding density of 6×10^4 cells/mL for 6 and 12 days. Total mRNA of MC3T3-E1 cells on the substrates was extracted (RNeasy Mini Kit, QIAGEN) and measured. The first strand of cDNA was synthesized from mRNA using SuperScript VILO cDNA Synthesis Kit (Invitrogen) with a BioRad iCycler following manufacturer's instructions. Early osteogenic marker (alkaline phosphatase, ALP), intermediate osteogenic markers (runt related transcription factor 2, Runx-2; and Osteopontin, OPN), and late osteogenic marker (osteocalcin, OC) were chosen as target genes for analysis. Glyceraldehyde-3-phosphate dehydrogenase (GAPDH) was used as an endogenous housekeeping gene. All the PCR reactions were performed on an Applied Biosystems StepOnePlus Real-Time PCR System in standard 10 μL reactions using EXPRESS SYBR GreenER qPCR SuperMix Kit (Invitrogen).

Surgical Procedures. The animals were used following the guidelines of the Ethical Committee for Animal Experiments of Tianjin Medical University. All in vivo work was done according to ref 38. A total of 60 implants (18 implants of each experimental group, and 36 implants for polished group) were implanted into the tibias of 18 New Zealand white rabbits (2–4 months of age), with a mean body weight of about 2.5–3 kg. Animals were anaesthetized by intramuscularly injection, and surgery was performed under sterile conditions. To reduce the peri-operative infection risk, the prophylactic antibiotic gentamicin was administered subcutaneously (15%, 0.1 ml/kg pre-operative and 0.15 ml/kg for 3 days postoperative, Heng Feng Qiang, Shanghai, China). Before the insertion of the implants, each animal was immobilized on its back. Subsequently, the hind limbs were shaved, washed, and disinfected with povidone–iodine. For implantation of the implant, a longitudinal incision was made on the medial surface of the left and right tibia. After exposure of the tibia, a 2.0 mm pilot hole was drilled until exposure to marrow, and drilling was performed with a gentle surgical technique, using low rotational drill speeds (800–1200 rpm) and continuous external cooling with saline. In this way, two bone cavities were created on the medial of the tibia. After preparation, the cavities were irrigated and the implants inserted, and the modified samples were seted in right tiba while the polished ones were in left as control. In each tibia, two implant sites were located, resulting in four implantation sites per rabbit. To ensure complete randomization, we placed the implants according to a balanced split-plot design. After insertion of the implants, the soft tissues were closed in separate layers, and the skin was closed transcutaneously. To reduce pain after surgery, all rabbits received Finadyne for 2 days postoperatively. To check the implant position, postoperative radiographs were taken. After an implantation period of 2 weeks, the rabbits were sacrificed by an overdose of Nembutal.

Subsequently, the implants with surrounding tissue were retrieved for histological and strength evaluation and micro-CT analysis.

Biomechanical Push-in Test. The biomechanical push-in test was used to assess the biomechanical strength of bone-implant integration.[15,17] Tibias containing a cylindrical implant were harvested after implantation for 2, 4, and 8 weeks and fixed on a steel fixture with the top surface of the implant being horizontal, bones on the back side of implants were cut off before the push-in test. The testing machine (Instron 5544 electromechanical testing system, Instron, Canton, MA) equipped with a 0.5 kN load cell and a pushing rod (0.8 mm diameter) was used to load the implant vertically downward at a crosshead speed of 1 mm/min. The push-in value was determined by measuring the peak of a load−displacement curve.

Histological Examination. The implants containing surrounding bone were cut down from the tibia by using a water-cooled diamond saw with the thickness of 0.25 mm (FALCON, China). After being fixed in 10% formalin for 7 days and dehydrated in serial concentrations of ethanol from 70% to 100%, the retrieved implants were embedded in methyl methacrylate and polymerized at 37 °C for a week. The nondecalcified sections, which were parallel to the long axis of the femur, were made on a diamond saw (Leica microtome, Germany) and grounded to about 20 μm in thickness. The sections were stained with toluidine-blue and then observed by light microscopy (Olympus Bx60, Japan).

Micro-CT Scan. To further investigate the in vivo differentiation of the different titanium implants, we performed an in vivo transplantation assay. The micro-CT scanner (SkyScan 1174) was used to determine the changes in bone mineral density (BMD) around the implants after 2, 4, and 8 weeks' implantation in rabbits. Specimens were scanned with a resolution of 6.5 μm; 260 scan slices were taken and reconstructed. The output was displayed as 3D stacks using CtVol (SkyScan). CTan software (Sky-Scan) was used to calculate BMD within 500 nm around implants, and the calibration was performed using HA as standard sample.

Statistical Analysis. Experiments were run in quintuplicate per sample. Standard deviations were plotted as error bars for the data points on all figures. For the majority of the data, the experimental error was found to be reasonable. Statistically significant differences were assessed by SAS6.12 during the in vitro and in vivo experiments. Difference with p values <0.05 were considered to be significant.

RESULTS AND DISCUSSION

Surface Analysis of FSL-Treated Samples. Figure 2a−c showed the surface structure of the different samples after FSL surface treatment. When laser fluence was 1.27 J/cm^2 (Figure 2b), the structure was composed by tiny islands of about 3 μm in diameter and pores of approximate 1 μm on the sample surface. When the laser fluence rose to 2.55 J/cm^2 (Figure 2c), tiny islands and caverns were interconnected to form a stripe of about 6 μm in width. With the analysis of AFM, a groove structure of about 4 μm in depth and 40 μm in width was found on the sample surface (Figure 2d). The groove surface was covered by a large number of peaks around 0.6 μm in height and 5−7 μm in diameter and the peak surface was covered with fine particles ranging from 50−500 nm in diameter. Calcium and phosphorus were detected on the Ti surface by the EDAX (Figure 2g). The interplanar spacing about 0.345 nm as shown in Figure 2f was equal to that of apatite. The selected area electron diffraction pattern (Figure 2i) indicated the existence of Ca/P phase. Therefore, the deposited Ca/P phase should be apatite. Figure 2h showed surface contour line of different samples. A periodic structure existed on 100Ti with about 10 μm in distance and 1.5 μm in depth. 200Ti and SLA samples showed 40-50 μm in periodic structure and 4 μm in depth on the surface. A large amount of protuberance with length of several micrometers existed in the periodic structure of sample surface processed by FSL of 1.27 and 2.55 J/cm^2, whereas SLA surface seemed even. In addition, on FSL-treated sample, surface groove showed a regular structure in parallel with laser processing direction, whereas the SLA surface presented out-of-order structure due to the random strike of sand grains. On the basis of SEM and AFM analysis, the FSL-induced surface patterns can be described as a regular tertiary structure: the first stage is the groove structure with 40 μm in width and 4 μm in depth; the second is the peak structure with 2−7 μm in diameter; and the third is the fine particles with 50−500 nm in diameter that covers the peak surface. It was anticipated that the large scale groove would be advantageous for cells to climb and small scale nanostructure would benefit adhesion of cell pseudopod.[10,11]

When FSL irradiated the sample surface, two-photon absorption occurred at the target surface, and the energy of photons was transferred to the electrons, which made the temperature of electrons soar.[39,40] Strenuous vibration of high-temperature electron started to interact with surrounding electrons and lattices, and transferred energy to surrounding electrons and lattices to increase integral temperature on sample surface. Because the speed of energy transfer in electrons and lattices was different,[39,41,42] the temperature of electron was much higher than that of lattice, and a temperature stress was produced between electron and lattice.[41,42] When the temperature stress was high enough to break lattice structure of crystals (that was, laser pulse energy reached damage threshold), the lattice on the sample surface started to break with partial high-energy atoms as well as electrons stripping from sample surface and splashing away at high speed. These high-energy particles collided with surrounding water molecules, which could produce plasma in the laser irradiation zone to cause ionizing.

On the other hand, high-temperature plasma caused sharp increase of solution temperature in the position of laser irradiation and brought vaporization, which made the surrounding calcium, phosphate ions aggregate rapidly to reach a high degree of supersaturation.[37] Subsequently, solid precipitation took place in the supersaturated solution. During the process of plasma extinction, bubble volume sharply shrank in vaporization position due to the decrease of temperature, thus neighboring solvent replaced these bubble positions rapidly and drove precipitated particles in the solution to sample surface. Meanwhile, when FSL irradiated titanium surface, oxide layer and hydroxyl adsorption layer on sample surface were removed, metal atoms within sample were exposed and showed high chemical activity. The exposed metal atoms reacted with various ions and particles in the solution such as phosphate radical and calcium ions.[35,36]

In Vitro Experiments. Cell attachment is an important factor to influence the cell-implant interactions, and it is critical in determining the initial success of an implant. Figure 3a showed cell numbers on different samples after culturing for 12 h. About 30% of the seeded cells attached to the polished Ti. On the surface of 100Ti, about 25% of the seeded cells attached, showing no obvious difference with the Ti sample (p = 0.075). On the surface of 200Ti, approximate 50% of the seeded cells attached, indicating an increase of about 60% over the polished Ti substrate (p = 0.015). The significantly higher cell number on 200Ti suggested that the laser treatment with certain parameters could increase cell adhesion.

Figure 3b−e showed the fluorescence images of MC3T3-E1 cells after 48 h culturing on different samples. On the polished Ti surface, there were fewer cells and most of them were in

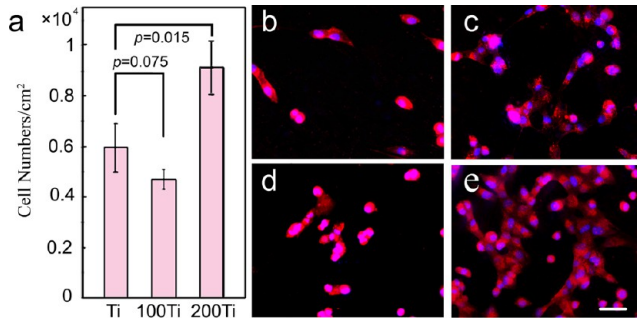

Figure 3. MC3T3-E1 cell numbers on samples after cultured for (a) 12 h and fluorescence images of cells after cultured for 48 h on different samples, (b) Ti, (c) SLA Ti, (d) 100Ti, and (e) 200Ti. In images b–e: red color represents the F-actin cytoskeleton of osteoblasts, and the nuclei of cells are in blue.

fusiform shape as usual, only some cells started to divide. On SLA sample surface, more cells were observed. Similar cell morphology was observed on the surface of 100Ti as that on polished Ti surface. While on the surface of 200Ti, the most cells were found and all the cells performed an active proliferation and division. It was in accordance with above cell adhesion behavior that cells preferred to attach and proliferate on the surface of 200Ti.

To further investigate the effect of micropatterns on cell differentiation at molecular level, we examined osteoblastic gene expressions of cells by real-time PCR after culturing for 6 and 12 days, respectively. After culturing cells for 6 days, there was no significant difference in ALP expression among the samples, as shown in Figure 4a ($p < 0.05$). However, on sample

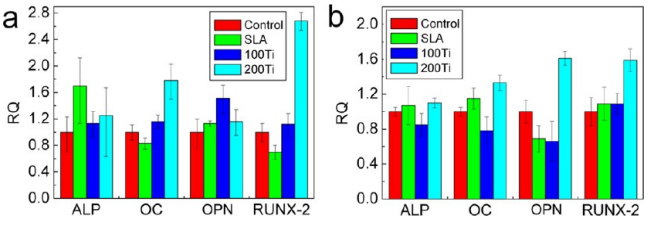

Figure 4. RT-PCR analysis of MC3T3-E1 cells cultured on different sample surfaces for (a) 6 and (b) 12 days. After culturing for 6 days, the difference of ALP expression among the samples is not significant ($p < 0.05$), whereas higher expression of Runx-2 and OC on sample 200Ti is observed ($p < 0.05$). After culturing for 12 days, all the expressions of Runx-2, OPN, and OC on 200Ti were the highest ($p < 0.05$).

200Ti, it showed much higher expression of Runx-2 and OC ($p < 0.05$). After culturing for 12 days, all the expressions of Runx-2, OPN, and OC on 200Ti were much higher than those on polished Ti and SLA Ti ($p < 0.05$), suggesting that the surface of 200Ti stimulated the cell differentiation most.

In Vivo Experiments. To examine the impact of FSL treatment on early osseointegration, we prepared cylindrical implants and implanted into rear leg tibia of New Zealand rabbit (Figure 5a, b). After 2, 4, and 8 weeks, push-in experiments (Figure 5c) were performed to analyze the binding capacity between implants and bone tissues. The typical push-in test curves and average binding forces were shown in Figure 5d-i. It can be seen that the FSL-treated sample exhibited a superior binding capacity with bone tissue than that of the polished and SLA samples during the first 8 weeks after implantation. After 2 weeks, FSL-treated sample had a binding capacity of 18.6 N with bone tissues, which was significantly higher than that of the polished Ti (2.5 N) and SLA samples (5.3 N) (Figure 5d, g). With the prolonged time of implantation, the binding capacity between implant and bone tissue was strikingly elevated (Figure 5e, f, h, and i). When the implantation was prolonged to 8 weeks, the binding capacity between FSL-treated sample and bone tissue increased to 52.3 N, while that of the polished and SLA samples showed only 19.1 and 31.5 N, respectively (Figure 5f, i).

Figure 6 showed the fluorescence and toluidine blue dyeing observation at the interface after 8-week implantation for the analysis of binding status between the implant and the bone tissue. A layer of fibrous tissues grew on polished Ti and SLA Ti surfaces, whereas bone trabecula and a large amount of newly born bones were formed around FSL-treated implant. Stronger fluorescence density was observed on the FSL surface than on polished Ti and SLA implants, which demonstrated that newly born bone tissues grew much more energetically around FSL-treated implant than around polished Ti and SLA implants. The active growth of new bones on FSL-treated implant without evident fibrous tissue suggested good osseointegration between the FSL-treated implant and the bone tissues.

The binding property at the interface between the implant and the bone tissue at different time points was also analyzed by micro-CT. Figure 7 showed the three-dimensional reconfiguration. After 2 weeks of implantation, obvious gap presented at the interface of the bone tissue and polished Ti as well as SLA samples, while the growth of new bone tissue was observed on parts of FSL-treated surface. When it was implanted for 4 weeks, the gap between the bone tissue and polished Ti as well as SLA sample shrank, and new bone tissue started to grow on SLA surface. A fine osseointegration was found around FSL-treated sample with a rather compact bone tissue structure. When the implantation lasted for 8 weeks, no gaps could be seen between the bone tissue and all the implants. Bone tissue around FSL-treated sample was the most among the three samples, and cortical bone evidently grew towards medullary cavity interior of FSL-treated sample.

Based on the results of micro-CT, CTan software (Skyscan) was applied to calculate the average bone mineral density (BMD) of cortical bone with a boundary of 500 μm around implant. The results were also shown in Figure 7. Two weeks later, the average BMD of polished Ti, SLA, and FSL-treated samples was 0.43, 0.52, and 0.55 g/cm^3, respectively. Accompanying the prolonged implantation, the BMD around the samples increased gradually. When the implantation lasted for 8 weeks, the average values reached to 0.48, 0.56, and 0.61 g/cm^3 around different samples.

When the implant was inserted into the tibia of rabbit, the blood in the wound initially formed blood clotting around implant.[43] The research discovered that surface chemical constituents and microtopological structure of the sample exerted significant influence on blood response, and furthermore, determined subsequent ossification responses.[44,45] In this work, surface with rough micropatterns encouraged platelet aggregation and fibronectin adhesion, and then promoted attachment of osteoblast.[45] Meanwhile, partial dissolution of Ca/P phase on implant surface enhanced the concentration of Ca^{2+} and PO_4^{3-} ions around the implant, as shown in Figure 1. A 30–40 μm periodic structure of sample surface through the FSL treatment of 2.55 J/cm^2 facilitated adhesion of osteoblast

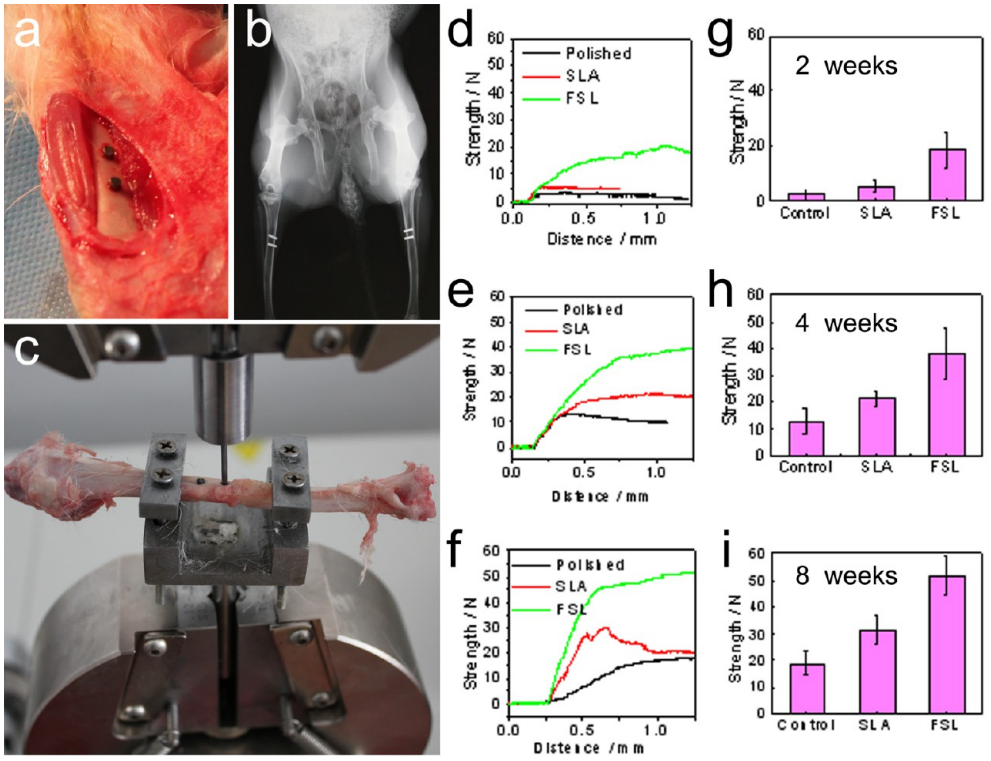

Figure 5. Surgical and push-in test. (a) Surgical process, (b) X-ray image, (c) push-in test; the push-in curves of samples at the time of (d) 2, (e) 4, and (f) 8 weeks; (g–i) the binding force between implants and bone. Polished is the control sample with a smooth surface, SLA is the sample treated with SLA method, and FSL is the sample treated with 2.55 J/cm^2 femtosecond laser. (p<0.05).

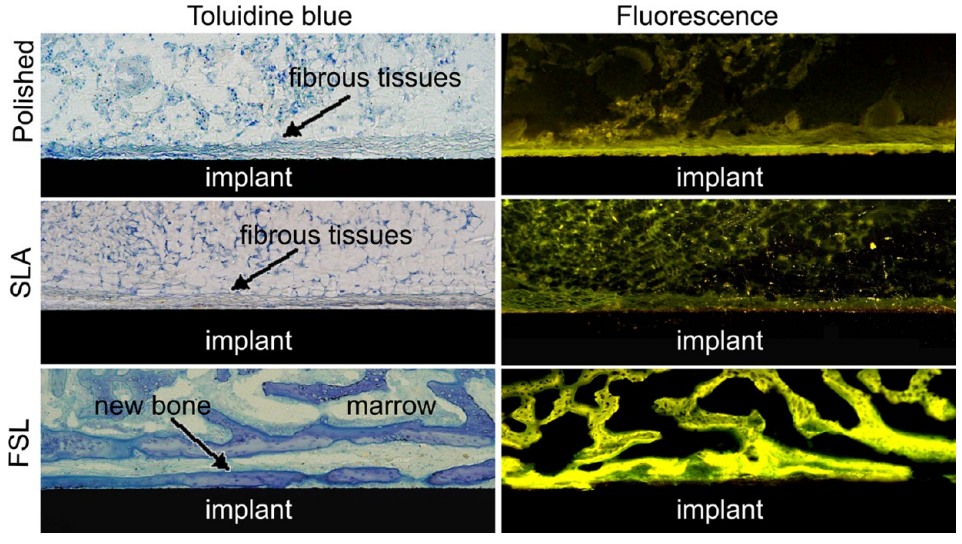

Figure 6. Toluidine blue dyeing and fluorescence images at the interface between the implant and the bone tissue after 8-week implantation.

on sample surface. When osteoblast adhered to implant surface, Ca^{2+} and PO_4^{3-} ions provided necessary substances for maturity and mineralization of osteoblast as well as the growth of new bone. The favorable growth of new bone tissue, higher BMD, and tighter connection between the implant and the bone tissue suggested that the hierachical micropattern and Ca/P deposition accelerated the early osseointegration, which has great potential used in orthopaedic fields.

CONCLUSION

Femtosecond laser was applied to create the hierachical micropattern as well as to deposit Ca/P phase on the surface of Ti implant at the same time. Enhanced MC3T3-E1 osteoblast adhesion and proliferation was observed on the surface of 200Ti. Also, higher expressions of osteogenic markers were detected on the surface of 200Ti after 12 days of cultivation. It indicated that 200Ti was favorable for cell adhesion, proliferation and differentiation. The in vivo studies showed that FSL-treated implants exhibited better osseointegration with bone tissue after 2-week implantation. Binding force of FSL-treated implants with tibia tissue was much higher than that of the polished and SLA Ti surfaces after implantation for 2, 4, and 8 weeks. Bone trabecula formed around FSL-treated implants without fibrous tissue. The average BMD

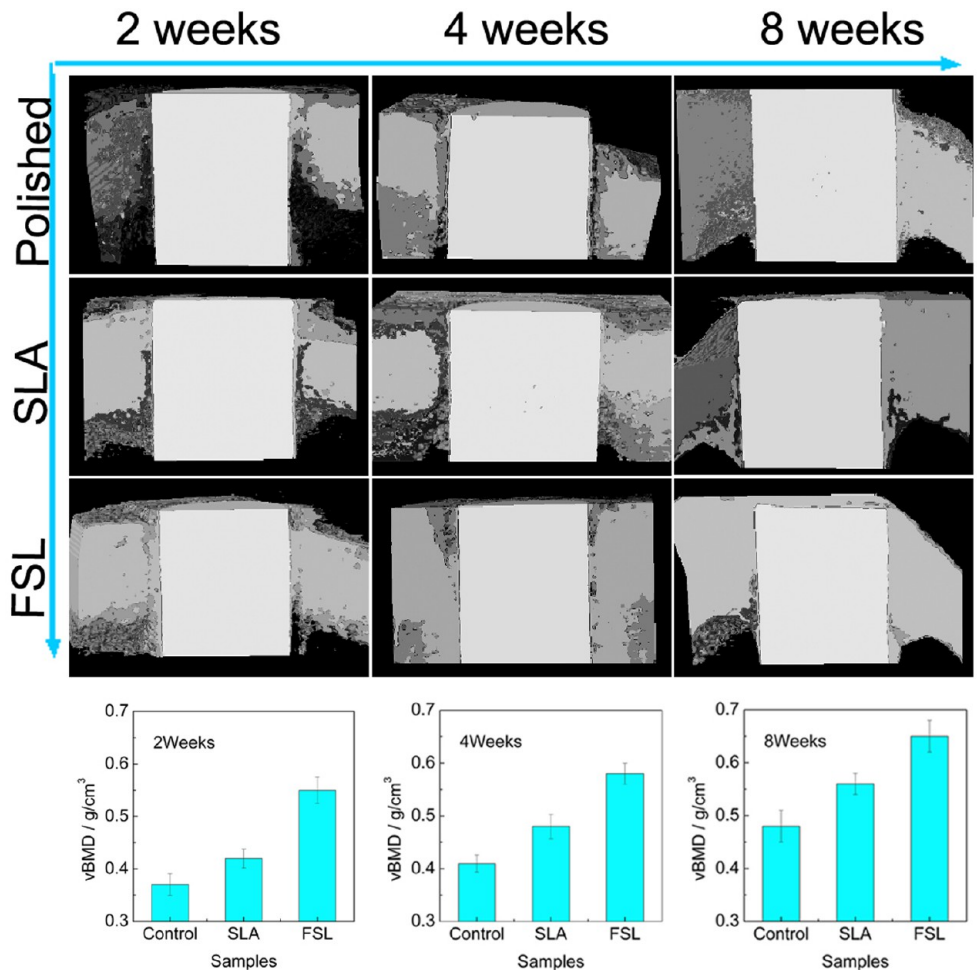

Figure 7. Reconstruction of implants based on Micro-CT and the BMD calculation of new bone around the implants ($p < 0.05$).

around FSL-treated implants was higher than that of polished and SLA Ti implants. Therefore, the FSL-treated implants could enhance osseointegration in the early stage of implantation.

AUTHOR INFORMATION

Corresponding Author

*E-mail: Liangchunyong@126.com (C. Liang); changyi_li@sina.com (C. Li); xjyang@tju.edu.cn (X. Yang).

Notes

The authors declare no competing financial interest.

ACKNOWLEDGMENTS

The authors gratefully acknowledge the support by the National Natural Science Foundation of China (Projects 50901029, 51171058, and 51201056)), Tianjin National Natural Science Foundation (Project 2JCZDJC20200), China Postdoctoral Science Foundation funded project (Project 2012M510841), Outstanding Youth Science and Technology Innovation Fund of Hebei University of Technology (Project 2011008), College Science Research Project of Hebei Province (Project Z2010124).

REFERENCES

(1) Balasundaram, G.; Sato, M.; Webster, T. J. *Biomaterials* **2006**, *27*, 2798−805.
(2) Miron, R. J.; Oates, C. J.; Molenberg, A.; Dard, M.; Hamilton, D. W. *Biomaterials* **2009**, *31*, 449−460.
(3) Oya, K.; Tanaka, Y.; Saito, H.; Kurashima, K.; Nogi, K.; Tsutsumi, H.; Tsutsumi, Y.; Doi, H.; Nomura, N.; Hanawa, T. *Biomaterials* **2009**, *30*, 1281−1286.
(4) Lee, D.-W.; Yun, Y.-P.; Park, K.; Kim, S. E. *Bone* **2012**, *50*, 974−982.
(5) Petersson, I. U.; Loberg, J. E. L.; Fredriksson, A. S.; Ahlberg, E. K. *Biomaterials* **2009**, *30*, 4471−4479.
(6) Wong, M. H.; Cheng, F. T.; Pang, G. K. H.; Man, H. C. *Mater. Sci. Eng., A* **2007**, *448*, 97−103.
(7) Man, H. C.; Wang, Q.; Guo, X. *Opt. Laser Eng.* **2010**, *48*, 583−588.
(8) Vrana, N. E.; Dupret-Bories, A.; Bach, C.; Chaubaroux, C.; Coraux, C.; Vautier, D.; Boulmedais, F.; Haikel, Y.; Debry, C.; Metz-Boutigue, M.-H.; Lavalle, P. *Biotechnol. Bioeng.* **2012**, *109*, 2134−2146.
(9) Lu, X.; Leng, Y.; Zhang, X.; Xu, J.; Qin, L.; Chan, C.-w. *Biomaterials* **2005**, *26*, 1793−1801.
(10) Divya Rani, V. V.; Vinoth-Kumar, L.; Anitha, V. C.; Manzoor, K.; Deepthy, M.; Shantikumar, V. N. *Acta Biomater.* **2012**, *8*, 1976−1989.
(11) Wu, Y.; Zitelli, J. P.; TenHuisen, K. S.; Yu, X.; Libera, M. R. *Biomaterials* **2011**, *32*, 951−960.
(12) Lim, Y. C.; Johnson, J.; Fei, Z.; Wu, Y.; Farson, D. F.; Lannutti, J. J.; Choi, H. W.; Lee, L. J. *Biotechnol. Bioeng.* **2011**, *108*, 116−126.
(13) Schwartz, Z.; Olivares-Navarrete, R.; Wieland, M.; Cochran, D. L.; Boyan, B. D. *Biomaterials* **2009**, *30*, 3390−3396.
(14) Zhao, L.; Mei, S.; Chu, P. K.; Zhang, Y.; Wu, Z. *Biomaterials* **2010**, *31*, 5072−5082.

(15) Wang, N.; Li, H.; Lu, W.; Li, J.; Wang, J.; Zhang, Z.; Liu, Y. *Biomaterials* **2011**, *32*, 6900−6911.
(16) Zhang, X. N. *Adv. Mater. Res.* **2007**, *29-30*, 51−54.
(17) Balasundaram, G.; Sato, M.; Webster, T. J. *Biomaterials* **2006**, *27*, 2798−2805.
(18) Mirhosseini, N.; Crouse, P. L.; Schmidth, M. J. J.; Li, L.; Garrod, D. *Appl. Surf. Sci.* **2007**, *253*, 7738−7743.
(19) Khosroshahi, M. E.; Mahmoodi, M.; Tavakoli, J. *Appl. Surf. Sci.* **2007**, *253*, 8772−8781.
(20) Pfeifer, R.; Herzog, D.; Hustedt, M.; Barcikowski, S. *J. Mater. Proces. Technol.* **2010**, *210*, 1918−1925.
(21) Tsukamoto, M.; Asuka, K.; Nakano, H.; Hashida, M.; Katto, M.; Abe, N.; Fujita, M. *Vacuum* **2006**, *80*, 1346−1350.
(22) Vorobyev, A. Y.; Guo, C. *Appl. Surf. Sci.* **2007**, *253*, 7272−7280.
(23) Verma, A.; Sharma, A.; Kulkarni, G. U. *Small* **2011**, *7*, 758−765.
(24) Kolesnikova, T. A.; Kohler, D.; Skirtach, A. G.; Mohwald, H. *ACS Nano* **2012**, *6*, 9585−9595.
(25) Sada, T.; Fujigaya, T.; Niidome, Y.; Nakazawa, K.; Nakashima, N. *ACS Nano* **2011**, *5*, 4414−4421.
(26) Nedyalkov, N. N.; Miyanishi, T.; Obara, M. *Appl. Surf. Sci.* **2007**, *253*, 6558−6562.
(27) Borowiec, A.; Haugen, H. K. *Appl. Phys. Lett.* **2003**, *82*, 4462−4464.
(28) Mathieu, M.; Schunk, D.; Franzka, S.; Mayer, C.; Hasselbrink, E.; Hartmann, N. *Small* **2009**, *5*, 2099−2104.
(29) Scheres, L.; Klingebiel, B.; Maat, J. t.; Giesbers, M.; de Jong, H.; Hartmann, N.; Zuilhof, H. *Small* **2010**, *6*, 1918−1926.
(30) Liang, C.; Yang, Y.; Wang, H.; Yang, J.; Yang, X. *Chin. Sci. Bull.* **2008**, *53*, 700−705.
(31) Yang, Y.; Yang, J.; Liang, C.; Wang, H.; Zhu, X.; Kuang, D.; Yang, Y. *Appl. Phy. A: Mater. Sci. Process.* **2008**, *92*, 635−642.
(32) Yang, Y.; Yang, J.; Liang, C.; Wang, H. *Opt. Exp.* **2008**, *16*, 11259−11265.
(33) Symietz, C.; Lehmann, E.; Gildenhaar, R.; Kruger, J.; Berger, G. *Acta Biomater.* **2010**, *6*, 3318−3324.
(34) Symietz, C.; Lehmann, E.; Gildenhaar, R.; Koter, R.; Berger, G.; Krüger, J. *Appl. Surf. Sci.* **2011**, *257*, 5208−5212.
(35) Wang, H.; Liang, C.; Yang, Y.; Li, C. *Biomed. Mater.* **2010**, *5*, 054115.
(36) Liang, C.-Y.; Wang, H.-S.; Yang, Y.; Yang, J.-J.; Chen, G.-F.; Li, C.-Y. *Chin. Phys. B* **2010**, *19*, 094208.
(37) Yang, Y.; Yang, J.; Liang, C.; Wang, H.; Zhu, X.; Zhang, N. *Opt. Exp.* **2009**, *17*, 21124−21133.
(38) Schouten, C.; van den Beucken, J. J.; de Jonge, L. T.; Bronkhorst, E. M.; Meijer, G. J.; Spauwen, P. H.; Jansen, J. A. *Biomaterials* **2009**, *30*, 6407−6417.
(39) Povarnitsyn, M. E.; Itina, T. E.; Sentis, M.; Khishchenko, K. V.; Levashov, P. R. *Phys. Rev. B* **2007**, *75*, 235414.
(40) Serbin, J.; Egbert, A.; Ostendorf, A.; Chichkov, B. N.; Houbertz, R.; Domann, G.; Schulz, J.; Cronauer, C.; Frolich, L.; Popall, M. *Opt. Lett.* **2003**, *28*, 301−303.
(41) Chichkov, B. N.; Momma, C.; Nolte, S.; von Alvensleben, F.; Tünnermann, A. *Appl. Phys. A: Mater. Sci. Process.* **1996**, *63*, 109−115.
(42) Fujimoto, J. G.; Liu, J. M.; Ippen, E. P.; Bloembergen, N. *Phys. Rev. Lett.* **1984**, *53*, 1837−1840.
(43) Slaets, E.; Carmeliet, G.; Naert, I.; Duyck, J. *J. Periodontol.* **2006**, *77*, 1015−1024.
(44) Park, J. Y.; Gemmell, C. H.; Davies, J. E. *Biomaterials* **2001**, *22*, 2671−2682.
(45) Thor, A.; Rasmusson, L.; Wennerberg, A.; Thomsen, P.; Hirsch, J.-M.; Nilsson, B.; Hong, J. *Biomaterials* **2007**, *28*, 966−974.